Unmanned Systems, Available online 6 May 2023
DOI: 10.1142/S2301385024500298

$\mathcal{L}_1$ Adaptive Path-following of Airships in Wind

Toufik Souanef[a] James Whidborne[a] and Shi Qian Liu[b]

[a] *Cranfield University, College Road, Cranfield, United Kingdom* [b] *Shanghai Jiao Tong University, China*
E-mail: toufik.souanef@cranfield.ac.uk

This paper proposes an adaptive, three dimensional (3D) path-following controller for airships in the presence of wind disturbances, which explicitly considers that wind speed is time-varying. The main idea is to formulate airship path-following as control design for systems in the presence of parametric uncertainties and external disturbances. Assuming that there is no prior information on wind, the proposed solution is based on the $\mathcal{L}_1$ adaptive controller. This approach makes clear statements for performance specifications of the controller and relaxes the common assumption that wind speed is constant. This makes the design more realistic and the analysis more rigorous, because in practice, the wind speed may be time varying. The results of the simulation indicate that the path following system has a good performance and is robust against wind disturbances.

Keywords: Airship Path-Following; Airship Control; $\mathcal{L}_1$ Adaptive Control

1. Introduction

Stratospheric airships, like other unmanned aerial vehicles, have potential military and civilian applications such as observation, remote sensing and communication relay platforms, to cite a few [1, 2]. Many applications require airships to autonomously follow a desired trajectory. However, considering the slow dynamics and the poor maneuverability of airships, the path-following control strategy is more practical than trajectory tracking in terms of controller design since no strict temporal requirement exists [3]. Furthermore, path-following rather than trajectory tracking is more appropriate for most vehicles because in the presence of constant wind, optimal engine performance is relative to the moving air, not to the earth frame. This allows the aircraft to maximize range, and speed is controlled separately.

Autonomous path-following is a challenge for airships, because they are underactuated, which means that the sway and heave motions cannot be controlled directly, especially when hovering. This is a direct consequence of the loss of aerodynamic forces of control surfaces. [4, 5]. Furthermore, due to the characteristics of their large volume, slow speed and low-maneuverability, airship motion is sensitive to wind [6,7]. Actually, in the stratosphere, deviations from the mean behaviour of the winds occur during events called sudden warmings, when the meridional temperature gradient reverses on timescales as short as several days. This also has the effect of reversing the zonal wind direction [8]. If the path-following controller does not account for wind, the path tracking ability of airships will be reduced. Therefore, there is a need to design path-following methods that are robust against wind disturbances.

Several results on path-following control for airships have been presented in recent years. A path-following controller for airships was proposed using H_∞ and PI control [9]. A path following control design has been developed by linearizing the dynamic model, which only works effectively near the equilibrium point [10]. A global planar path-following for stratospheric airships was proposed based on guidance integrated backstepping control in [11]. A sliding mode control for an autonomous unmanned airship has also been proposed [12]. A backstepping controller for the path following control problem of airships based on the nonlinear models considering external disturbance and actuators saturation was also proposed [13]. A command filtered backstepping controller using the guidance-based path-following principle for an underactuated stratospheric airship was proposed [14]. A path following controller based on backstepping and PD control technique is presented in [15], the guidance vector is constructed to obtain the desired attitude angles and velocity. A gain-scheduling controller with step-by-step design for airship path following under wind disturbances was proposed [16]. More recently, a virtual guidance-based finite-time adaptive neural backstepping path-following control approach was proposed for underactuated autonomous airship with error constraints and uncertainties [17]. The planar path following control problem for an autonomous airship was investigated taking actuator saturation, actuator dynamics, parameter variation, and wind field into account [18]. The proposed solution was based on a command filtered backstepping controller combined with nonlinear disturbance observer. A Lyapunov-based guidance law with the sideslip and attack angle compensation was designed [19], which decreases the

path-following steady-state error.

However, all these approaches either do not explicitly consider wind or they assume wind speed to be constant (steady wind), which is not realistic as mentioned above. Based on the design idea of the line-of-sight (LOS) guidance law, a parameter-observer-based LOS (POBLOS) guidance law has been proposed [20]. The unknown and time-varying influence from the wind was estimated by the parameter observer and then compensated in the design of the guidance loop. The paper only examines paths in 2D, while, in the presence of wind disturbance, it would be more appropriate to consider 3D path-following.

An alternative solution can be provided through the use of $\mathcal{L}_1$ adaptive control [21]. $\mathcal{L}_1$ adaptive control has been applied for various flight control systems [22–25] to cite a few. The benefit of $\mathcal{L}_1$ adaptive control is its capacity for fast and robust adaptation that leads to desired transient performance for both system signals, input and output. These characteristics make it suitable for systems subject to external time-varying disturbances, such as airships motion in wind.

In this paper we formulate the problem of 3D path-following of airships as a control systems design problem in the presence of parametric uncertainties and external disturbances. The approach was first presented for small fixed-wing UAVs path-following in wind [26] . Assuming that wind is time-varying, the proposed solution is based on a new design of the $\mathcal{L}_1$ adaptive controller based on sliding mode control.

The advantage of the sliding mode adaptation is that it can show the formal proof of asymptotic convergence of the prediction error and the performance bounds. However [26] addressed only the problem of planar 2D paths. Actually, considering 3D path-following through general paths is more appropriate. This is particularly true when taking atmospheric disturbances into account [27].

The contributions of the paper are:

- Formulation of the 3D path-following problem as a control design problem in the presence of unknown uncertainties and external disturbances.
- Development of an $\mathcal{L}_1$ adaptive path-following controller that is robust against time-varying wind disturbances.
- Proof of asymptotic stability of the system using sliding mode adaptation.
- Demonstration of the performance of the proposed controller in simulations.

The rest of this paper is organized as follows: Section 2 formulates the path following problem. In section 3, the design of the path following system is presented. Section 4 gives the stability analysis of the control system. The results of simulations are given and the performance of the path following system is evaluated in section 5. In the last section, a brief summary is presented with some concluding remarks.

2. Problem Formulation

The kinematic model of an airship is similar to fixed-wing aircraft in the inertial frame and is given from [28, p.24] as follows

$$\begin{aligned} \dot{p}_n &= V_a\ \cos(\psi)\ \cos(\gamma_a) + W_n, \\ \dot{p}_e &= V_a\ \sin(\psi)\ \cos(\gamma_a) + W_e, \\ \dot{p}_d &= -V_a\ \sin(\gamma_a) + W_d, \end{aligned} \tag{1}$$

where p_n, p_e, p_d are respectively the North, East and down (negative of the altitude) positions, V_a is the airspeed, ψ is the heading angle relative to the north, γ_a is the air referenced flight path angle, and W_n, W_e, and W_d are wind speeds in the inertial frame. This model is derived under the assumption that the airship is in steady level flight. In this case, the airspeed V_a is aligned with the x-direction of the body frame, which means that the sideslip angle β is zero.

Furthermore, the kinematic equation of motion for the heading angle is given by

$$\dot{\psi} = r, \tag{2}$$

where r is the heading rate.

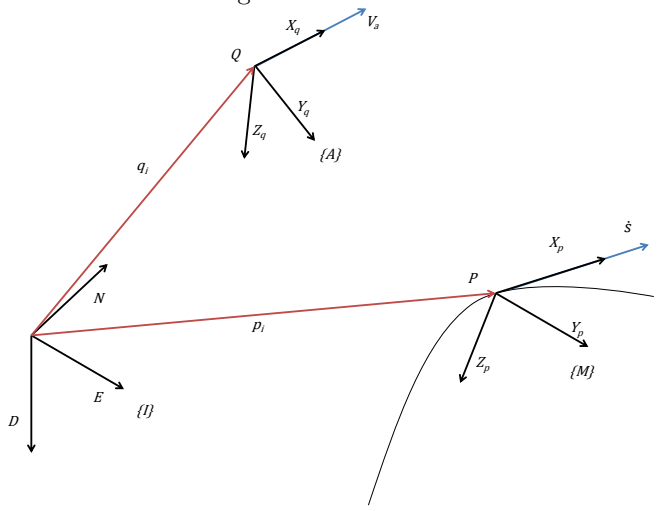

Fig. 1. Curved Path-Following Frames.

Assumption 1. The airship is equipped with an attitude (inner-loop) controller that is robust against forces and couples resulting from wind. Therefore, the objective is to compute the flight path angle and heading rate angle commands to the autopilot to maintain the airship on the desired path despite the presence of wind.

Assumption 2. There is no available information on the wind, neither its velocity nor its direction.

In Fig. 1, Q defines the position of the centre of volume of the airship, with coordinates $q_i = [x_q, y_q, z_q]^\top$ in the inertial frame $\mathcal{I}$. The moving orthonormal frame $\mathcal{M}$, is referenced by the speed vector of the virtual target [29]. This frame is completely different from the Serret-Frenet frame [30]. P defines the position of the virtual target,

moving on the desired path, which is the origin of $\mathcal{M}$, with coordinates $p_i = [x_p, y_p, z_p]^\top$ in the inertial frame $\mathcal{I}$.

The idea is to minimize the position error of the airship relative to the virtual target, and so maintain the airship on the reference path despite the presence of wind disturbances.

Remark 1. In this paper the notation showing time dependence of the variables $\cdot(t)$ is dropped unless it is not clear from the context.

In the following, the mathematical model of the three-dimensional curved path-following is derived.

The virtual target inertial kinematic model at position p_i is defined as

$$\begin{aligned} \dot{x}_p &= \dot{l}\ \cos(\psi_p)\ \cos(\gamma_p), \\ \dot{y}_p &= \dot{l}\ \sin(\psi_p)\ \cos(\gamma_p), \\ \dot{z}_p &= -\dot{l}\ \sin(\gamma_p), \end{aligned} \tag{3}$$

where $[\dot{x}_p, \dot{y}_p, \dot{z}_p]$ are the coordinates of the velocity vector $\dot{p}_i$ in the inertial frame $\mathcal{I}$, $\dot{l}$ is the speed of the virtual target, l is the length of the path, ψ_p is the path heading angle and γ_p is the flight path angle.

The orientation of the desired path at position p_i can be characterized as

$$\begin{aligned} \psi_p &= \operatorname{atan2}(\dot{y}_p, \dot{x}_p), \\ \gamma_p &= -\arctan\left(\dot{z}_p / \sqrt{\dot{x}_p^2 + \dot{y}_p^2}\right). \end{aligned} \tag{4}$$

where $[\dot{x}_p, \dot{y}_p, \dot{z}_p]$ are the coordinates of the velocity vector $\dot{p}_i$ in the inertial frame $\mathcal{I}$.

Assumption 3. The roll angle of the airship is very small compared to the heading and flight path angles, such that it can be neglected, i.e. $\phi \approx 0$.

The position error e_m of the airship expressed in the moving frame $\mathcal{M}$, can be written as

$$e_m = T_{mi}(q_i - p_i), \tag{5}$$

where p_i q_i are, respectively, the position vector of the airship and the virtual target expressed in the inertial frame $\mathcal{I}$, and $T_{mi} = T_2(\gamma_p)T_3(\psi_p)$ is the transformation matrix from the inertial frame $\mathcal{I}$, to the moving frame $\mathcal{M}$, defined by

$$T_{mi} = \begin{bmatrix} \cos\gamma_p\ \cos\psi_p & \cos\gamma_p\ \sin\psi_p & -\sin\gamma_p \\ -\sin\psi_p & \cos\psi_p & 0 \\ \sin\gamma_p\ \cos\psi_p & \sin\gamma_p\ \sin\psi_p & \cos\gamma_p \end{bmatrix}. \tag{6}$$

Taking the time derivative of equation (5), yields

$$\dot{e}_m = T_{mi}(\dot{q}_i - \dot{p}_i) - \omega_{mi}^m \times T_{mi}(q_i - p_i), \tag{7}$$

where $\times$ denotes the cross product, and ω_{mi}^m is the angular rate of the moving frame $\mathcal{M}$ with respect to the inertial frame $\mathcal{I}$ resolved in the moving frame $\mathcal{M}$. Hence

$$\dot{e}_m = T_{mi}\dot{q}_i - \dot{p}_m - \omega_{mi}^m \times e_m, \tag{8}$$

where $\dot{p}_m$ is the velocity vector of the virtual target in the moving frame $\mathcal{M}$ defined by

$$\dot{p}_m = \begin{bmatrix} \dot{l} \\ 0 \\ 0 \end{bmatrix}. \tag{9}$$

In order to expand equation (8), the expression of the angular rate ω_{mi}^m can be written as follows

$$\omega_{mi}^m = \begin{bmatrix} 0 \\ \dot{\gamma}_p \\ 0 \end{bmatrix} + \begin{bmatrix} \cos\gamma_p & 0 & -\sin\gamma_p \\ 0 & 1 & 0 \\ \sin\gamma_p & 0 & \cos\gamma_p \end{bmatrix} \begin{bmatrix} 0 \\ 0 \\ \dot{\psi}_p \end{bmatrix} = \begin{bmatrix} -\dot{\psi}_p \sin\gamma_p \\ \dot{\gamma}_p \\ \dot{\psi}_p \cos\gamma_p \end{bmatrix}. \tag{10}$$

We also have

$$\dot{\psi}_p = \frac{d\psi_p}{dl}\frac{dl}{dt}, \tag{11}$$

and from equation (4) that

$$\psi_p = \operatorname{atan2}(y_p', x_p'), \tag{12}$$

where $x_p' = \frac{dx_p(l)}{dl}$ and $y_p' = \frac{dy_p(l)}{dl}$. Hence

$$\begin{aligned} \dot{\psi}_p &= \dot{l}\ \frac{d}{dl}\Big(\operatorname{atan2}\big(y_p', x_p'\big)\Big), \\ &= \dot{l}\, c_1(l), \end{aligned} \tag{13}$$

where $c_1(l) = \big(x_p' y_p'' - y_p' x_p''\big)/\big(x_p'^2 + y_p'^2\big)$, $x_p'' = \frac{d^2 x_p(l)}{dl^2}$ and $y_p'' = \frac{d^2 y_p(l)}{dl^2}$.

Similarly, it can be also shown that

$$\dot{\gamma}_p = \dot{l}\, c_2(l), \tag{14}$$

where $c_2(l) = \frac{(z_p''(x_p'^2 + y_p'^2) - z_p'(x_p' x_p'' + y_p' y_p''))}{(x_p'^2 + y_p'^2 + z_p'^2)(x_p'^2 + y_p'^2)^{1/2}}$ and $z_p'' = \frac{d^2 z_p(l)}{dl^2}$. Consequently, the system in (8) can be expanded as

$$\begin{aligned} \begin{bmatrix} \dot{x}_e \\ \dot{y}_e \\ \dot{z}_e \end{bmatrix} =& T_{mi} \begin{bmatrix} \dot{x}_q \\ \dot{y}_q \\ \dot{z}_q \end{bmatrix} - \begin{bmatrix} \dot{l} \\ 0 \\ 0 \end{bmatrix} \\ &- \begin{bmatrix} 0 & -\dot{l}\, c_1(l)\cos\gamma_p & \dot{l}\, c_2(l) \\ \dot{l}\, c_1(l)\cos\gamma_p & 0 & \dot{l}\, c_1(l)\sin\gamma_p \\ -\dot{l}\, c_2(l) & -\dot{l}\, c_1(l)\sin\gamma_p & 0 \end{bmatrix} \begin{bmatrix} x_e \\ y_e \\ z_e \end{bmatrix}, \end{aligned} \tag{15}$$

where (x_e, y_e, z_e) are the coordinates of e_m.

Therefore, the model in (1) can be written as

$$\begin{bmatrix} \dot{x}_q \\ \dot{y}_q \\ \dot{z}_q \end{bmatrix} = T_{ia} \begin{bmatrix} V_a \\ 0 \\ 0 \end{bmatrix} + \begin{bmatrix} W_n \\ W_e \\ W_d \end{bmatrix}, \tag{16}$$

where $T_{ia} = T_3(-\psi)\, T_2(-\gamma_a)$ is the transformation matrix from the airspeed referenced frame $\mathcal{A}$ to the inertial frame $\mathcal{I}$ defined by

$$T_{ia} = \begin{bmatrix} \cos\gamma_a\ \cos\psi & -\sin\psi\ \sin\gamma_a\ \cos\psi \\ \cos\gamma_a\ \sin\psi & \cos\psi\ \ \sin\gamma_a\ \sin\psi \\ -\sin\gamma_a & 0\ \ \cos\gamma_a \end{bmatrix}. \tag{17}$$

Hence

$$T_{mi}\begin{bmatrix}\dot{x}_q\\ \dot{y}_q\\ \dot{z}_q\end{bmatrix} = T_{ma}\begin{bmatrix}V_a\\ 0\\ 0\end{bmatrix} + \begin{bmatrix}V_x\\ V_y\\ V_z\end{bmatrix}, \tag{18}$$

where

$$\begin{bmatrix}V_x\\ V_y\\ V_z\end{bmatrix} = T_{mi}\begin{bmatrix}W_n\\ W_e\\ W_d\end{bmatrix},$$

and $T_{ma} = T_{mi}\, T_{ia}$ is the transformation matrix from the airspeed referenced frame $\mathcal{A}$ to the moving frame $\mathcal{M}$ defined by

$$\begin{aligned}T_{ma} &= T_2(\gamma_p)\, T_3(\psi_p)\, T_3(-\psi)\, T_2(-\gamma_a)\\ &= T_2(\gamma_p)\, T_3(-\psi_e)\, T_2(-\gamma_a)\\ &= \begin{bmatrix} C\gamma_p\, C\gamma_a\, C\psi_e + S\gamma_p\, S\gamma_a & -C\gamma_p\, C\psi_e\, C\gamma_p\, S\gamma_a\, C\psi_e - S\gamma_p\, C\gamma_a\\ C\gamma_a\, S\psi_e & C\psi_e & S\gamma_a\, S\psi_e\\ S\gamma_p\, C\gamma_a\, C\psi_e - C\gamma_p\, S\gamma_a & -C\gamma_p\, S\psi_e\ S\gamma_p\, S\gamma_a\, C\psi_e + C\gamma_p\, C\gamma_a\end{bmatrix},\end{aligned}$$

with $\psi_e = \psi - \psi_p$, $C \triangleq \cos$ and $S \triangleq \sin$. Substituting (18) in (15) it follows that

$$\begin{aligned}\dot{x}_e =& V_a\, C\gamma_p\, C\psi_e\, C\gamma_a + V_a\, S\gamma_p\, S\gamma_a\\ &- \big(1 - c_1(l)\, C\gamma_p\, y_e + c_2(l)\, z_e\big)\dot{l} + V_x,\\ \dot{y}_e =& V_a\, S\psi_e\, C\gamma_a - \big(c_1(l)\, C\gamma_p\, x_e + c_1(l)\, S\gamma_p\, z_e\big)\dot{l} + V_y,\\ \dot{z}_e =& V_a\, S\gamma_p\, C\psi_e\, C\gamma_a - V_a\, C\gamma_p\, S\gamma_a\\ &+ \big(c_2(l)\, x_e + c_1(l)\, S\gamma_p\, y_e\big)\dot{l} + V_z\\ \dot{\psi}_e =& r - c_1(l)\dot{l}.\end{aligned} \tag{19}$$

The objective is to compute the desired speed of the virtual target $\dot{l}$, the commanded heading rate $r_c = r$ and the air referenced flight path angle $\gamma_c = \gamma_a$ that maintain the airship on the desired path, despite the presence of wind. The proposed method is based on $\mathcal{L}_1$ adaptive control.

Remark 2. The use of the notations r_c and γ_c is justified by the fact that, in practice, these angles are the reference inputs for the attitude controller.

Letting $x = [x_e, y_e, z_e, \psi_e]^\top$ and $u = [r_c, \gamma_c, \dot{l}]^\top = [u_1, u_2, u_3]^\top$, equation (19) can be written in a compact form as follows

$$\dot{x} = f(x,u) + \zeta(t), \tag{20}$$

where

$$f(x,u) = \begin{bmatrix} V_a C\gamma_p C x_4 C u_2 + V_a S\gamma_p S u_2 - \big(1 - c_1(l) C\gamma_p x_2 + c_2(l) x_3\big) u_3\\ V_a S x_4 C u_2 - \big(c_1(l) C\gamma_p x_1 + c_1(l) S\gamma_p x_3\big) u_3\\ V_a S\gamma_p C x_4 C u_2 - V_a C\gamma_p S u_2 + \big(c_2(l) x_1 + c_1(l) S\gamma_p x_2\big) u_3\\ u_1 - c_1(l) u_3\end{bmatrix}$$

and

$$\zeta(t) = \begin{bmatrix}V_x(t)\\ V_y(t)\\ V_z(t)\\ 0\end{bmatrix}'$$

The system in equation (20) is a standard formulation of a nonlinear control system in the presence of external time-varying disturbances. The objective is to compute the control command $u(t)$ that stabilizes the system and maintains the airship on the desired path, despite the presence of wind. The proposed architecture is shown in Fig. 2.

3. Controller Design

A common procedure in adaptive control design is to linearize the nonlinear model at a given equilibrium or operating point, in order to develop a linear controller based on the linearized system model, and to augment the linear controller with the adaptive controller. This allows for better robustness of the system. Actually, it permits for less "burden" of the adaptive controller through the use of the prior knowledge of the input/output system [31].

In order to extract a linear model so that the inner loop can be simply stabilized, we assume a straight line trajectory. Thus

$$x_p'' = y_p'' = z_p'' = 0, \tag{21}$$

which implies that

$$c_1(l) = c_2(l) = 0. \tag{22}$$

So, for the equilibrium point $x_{eq} = [x_{1eq} \;\; x_{2eq} \;\; x_{3eq} \;\; 0]^\top$, $u_{eq} = [0 \;\; \gamma_p \;\; V_a]^\top$ and $\zeta_{eq} = 0$, where x_{1eq}, x_{2eq} and x_{3eq} are arbitrary, the linearized state space model of (20) is given for $\bar{x} = x - x_{eq}$, $\bar{u} = u - u_{eq}$ by

$$\dot{\bar{x}} = A_p \bar{x} + B_p \bar{u}, \tag{23}$$

where

$$A_p = \begin{bmatrix}0&0&0&0\\ 0&0&0&V_a\\ 0&0&0&0\\ 0&0&0&0\end{bmatrix}$$

and

$$B_p = \begin{bmatrix}0&0&-1\\ 0&0&0\\ 0&-V_a&0\\ 1&0&0\end{bmatrix}.$$

Hence, the non-linear system in (20) can be written as follows

$$\dot{x} = A_p x + B_p u + \tilde{f}, \tag{24}$$

where $\tilde{f}(x,u,t)$ is a nonlinear function that includes the higher order terms of the Taylor series expansion of $f(x,u)$ and the external disturbance $\zeta(t)$.

Remark 3. In practice the dynamics of the attitude controller are not negligible. As a consequence, we have the following

$$\begin{aligned}r =& F_1(s) r_c\\ \gamma =& F_2(s)\gamma_c,\end{aligned} \tag{25}$$

where $F_1(s)$ and $F_2(s)$ are unknown Laplace transfer functions.

Remark 4. It is important to underline that the matrices A_p and B_p are uncertain because it not possible in real flight conditions to maintain a constant airspeed V_a, especially in the presence of wind.

Consequently, the system in (24) can be written as

$$\dot{x} = A_m x + B\,\omega\,u + (A_p - A_m)x + \tilde{f}, \tag{26}$$

where $A_m = A - B\,K_p$ is a Hurwitz matrix of the desired dynamics of the system, A is the system dynamics matrix for the nominal airspeed, B is the input matrix of the system with the nominal airspeed, $K_p \in \mathbb{R}^{3\times 4}$ is the feedback matrix, and $\omega \in \mathbb{R}^{3\times 3}$ is an unknown gain matrix that contains the effect of the unknown dynamics of the attitude controller, the uncertainties resulting form the airspeed and the inner-loop controller dynamics.

For control design, the following approximation can be used

$$(A_p - A_m)x + \tilde{f}(t,x) = g(t,x), \tag{27}$$

where $g(t,x) \in \mathbb{R}^4$ is an unknown vector.

Consequently, the system in (26) leads to

$$\dot{x} = A_m x + B\omega u + g. \tag{28}$$

The resulting model makes straightforward application of the $\mathcal{L}_1$ adaptive controller that is described in the next section.

The block diagram of airship path-following in wind, based on $\mathcal{L}_1$ adaptive control, is illustrated in Fig. 2.

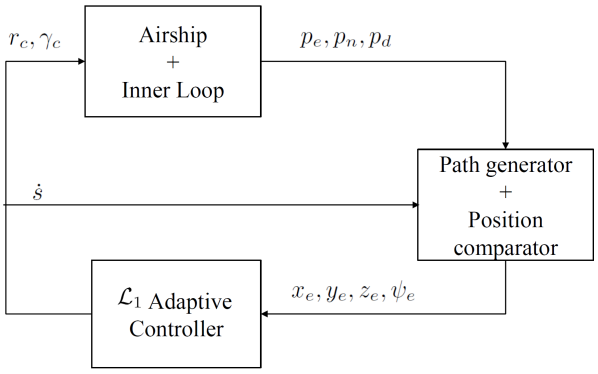

Fig. 2. $\mathcal{L}_1$ adaptive path-following control in wind.

The main advantage of the application of $\mathcal{L}_1$ adaptive control to airship path-following in wind is that good performance of the system can be obtained, whether the unknown wind velocity is constant or not [26]. This is a direct consequence of what was demonstrated in [32] that the $\mathcal{L}_1$ adaptive controller presents a good compromise between performance and robustness in the presence of disturbances with unknown bounds.

4. Sliding Mode based $\mathcal{L}_1$ Adaptive Controller for MIMO Systems

Given a class of MIMO systems defined by

$$\begin{aligned} \dot{x}(t) &= A_m x(t) + B\omega u(t) + g(t,x), \\ y(t) &= Cx(t), \qquad x(0) = x_0, \end{aligned} \tag{29}$$

where $A_m \in \mathbb{R}^{n\times n}$ is a known Hurwitz matrix that defines the desired dynamics of the system; $B^{n\times m}$, $C \in \mathbb{R}^{m\times n}$ are known constant matrices; $x(t) \in \mathbb{R}^n$ is the state vector which is assumed available through measurement; $u(t) \in \mathbb{R}^m$ is the control input vector; $y(t) \in \mathbb{R}^m$ is the output vector; $\omega \in \mathbb{R}^{m\times m}$ is an unknown constant matrix; and $g(t,x) \in \mathbb{R}^n$ is an unknown disturbance.

Assumption 5 There exist unknown real constants $L_1 > 0$ and $L_2 > 0$, such that for all $t \geq 0$ the following bounds hold:

$$\begin{aligned} \|g(t,x_1) - g(t,x_1)\|_\infty &\leq L_1\|x_1 - x_2\|_\infty \\ \|g(t,x)\|_\infty &\leq L_1\|x\|_\infty + L_2. \end{aligned}$$

This assumption is conventionally acceptable for real systems, given that an upper bound of disturbances, which the system may hold without being broken, is usually known from technical specifications or engineering insights.

Assumption 6 The system input gain matrix ω is assumed to be an unknown (non-singular) strictly row-diagonally dominant matrix with $\mathrm{sgn}(\omega_{ii})$ known. Also, it is assumed that there exists a known compact convex set Ω such that $\omega \in \Omega \subset \mathbb{R}^{m\times m}$.

4.1. *Controller Design*

In this section, a new design of the $\mathcal{L}_1$ adaptive control approach that borrows insights from sliding mode control to design the adaptive laws is presented. The main advantage compared to [27, 32] is that the bounds of the estimator derived in Lemma 2 are explicitly computed using the generalization of the Kantorovich inequality [33]. As a consequence, the performance and the robustness of the control system are computed without assuming a prior arbitrary small prediction error as it was proposed in [27].

As shown in Fig. 3, the $\mathcal{L}_1$ adaptive controller consists of three components: the state predictor, the adaptive law with fast adaptation, and the control law with a low-pass filter [21].

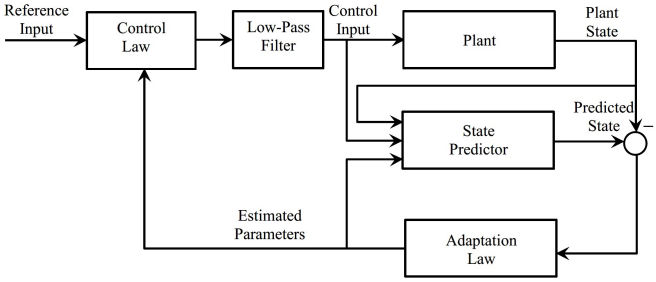

Fig. 3. The $\mathcal{L}_1$ adaptive controller.

The state predictor is defined as

$$\begin{aligned}\dot{\hat{x}}(t) &= A_m\hat{x}(t) + B\hat{\omega}(t)u(t) + \hat{\eta}(t),\\ \hat{y}(t) &= C\hat{x}(t), \qquad \hat{x}(0) = x_0,\end{aligned} \tag{30}$$

where $\hat{x}(t)$ is the predicted state and $\hat{\omega}(t)$ and $\hat{\eta}(t)$ are the estimates of the unknown system parameters and disturbances.

The sliding surface is defined as

$$\sigma(t) = \lambda\tilde{x}(t). \tag{31}$$

where $\tilde{x}(t) = \hat{x}(t) - x(t)$ is the state estimation error and $\lambda \in \mathbb{R}^{m\times n}$ is a constant arbitrary matrix, chosen such that λB is non-singular and the coefficients $\lambda(i,j) : i = 1\dots n; j = 1\dots m$ form a stable hyperplane.

The estimation of the disturbance $\eta(t,x)$ is defined by

$$\hat{\eta}(t) = \begin{cases} -(A_m + \rho\mathbb{I})\tilde{x}(t) - \big(\hat{L}_1(t)\|x\|_\infty \\ +\hat{L}_2(t)\big)\frac{\lambda^\top\sigma(t)}{\|\lambda^\top\sigma(t)\|}, & \text{if } \sigma(t)\neq 0,\\ 0 & \text{otherwise,}\end{cases} \tag{32}$$

where $\rho \in \mathbb{R}^+$ is an arbitrary real, and $\hat{L}_1(t)$ and $\hat{L}_2(t)$ are the estimations of the parameters L_1 and L_2, defined in Assumption 5, given by

$$\begin{aligned}\dot{\hat{L}}_1(t) &= \Gamma\|\sigma^\top(t)\lambda\|\|x\|_\infty,\ L_{10} = \hat{L}_1(0),\\ \dot{\hat{L}}_2(t) &= \Gamma\|\sigma^\top(t)\lambda\|,\ L_{20} = \hat{L}_2(0),\end{aligned} \tag{33}$$

where $\Gamma \in \mathbb{R}^+$ is the adaptation rate.

The input gain matrix ω is estimated by

$$\dot{\hat{\omega}}(t) = -\Gamma\ \mathrm{Proj}\big(\hat{\omega}(t), u(t)\,\sigma^\top(t)\lambda\, B\big)^\top. \tag{34}$$

The control law is given by

$$u(s) = KD(s)\Big(K_g\, r(s) - \hat{\nu}_1(s) - \hat{\nu}_2(s)\Big), \tag{35}$$

where $D(s)$ is an $m\times m$ strictly proper Laplace transfer function matrix; $K \in \mathbb{R}^{m\times m}$; $K_g = -(CA_m^{-1}B)^{-1}$ is the pre-filter of the MIMO control law; $\hat{\nu}_1(s)$ is the Laplace transform of $\hat{\nu}_2(t) = \hat{\omega}(t)u(t)$; $H_m(s) = C(s\mathbb{I} - A_m)^{-1}B$; $H_0(s) = C(s\mathbb{I} - A_m)^{-1}$; and $\hat{\nu_2} = H_m^{-1}(s)H_0(s)\hat{\eta}(s)$.

The design of $D(s)$ and K should lead to a strictly proper and stable filter transfer function matrix

$$F(s) = \omega KD(s)(\mathbb{I} + \omega KD(s))^{-1}, \tag{36}$$

with DC gain $F(0) = \mathbb{I}$.

Let

$$H(s) = (s\mathbb{I} - A_m)^{-1}b \text{ and } G(s) = H(s)\big(1 - C(s)\big). \tag{37}$$

The design of $F(s)$ needs to ensure the following $\mathcal{L}_1$-norm condition

$$\|G(s)\|_{\mathcal{L}_1}L_1 < 1. \tag{38}$$

For a particular class of systems, a possible choice for $D(s)$ might be $D(s) = (1/s)\mathbb{I}$ which yields a strictly proper $F(s)$ of the form

$$F(s) = \omega K(s\mathbb{I} + \omega K)^{-1}. \tag{39}$$

4.2. *Controller Analysis*

In this section, the performance of the $\mathcal{L}_1$ adaptive controller is analysed. More specifically it is shown that:

- The reference model resulting from perfect knowledge of the uncertainties and a corresponding non-adaptive controller is stable, subject to some conditions involving the filter $F(s)$.
- The prediction error, i.e. the error between the state of the plant and those of the state predictor, is uniformly bounded and asymptotically stable.
- The difference between the states/input of the system and those of the reference system is proportional to the prediction error.

The reference system, i.e. the closed-loop system with nominal parameters, is defined by

$$\begin{aligned}\dot{x}_r(t) &= A_m x_r(t) + B\omega u_r(t) + \eta_r(t, x_r),\\ y_r(t) &= Cx_r(t), \qquad x_r(0) = x_0.\end{aligned} \tag{40}$$

The reference control law is given by

$$u_r(s) = \omega^{-1}F(s)\Big(K_g r(s) - \nu_r(s)\Big), \tag{41}$$

where $\nu_r(s) = H_m^{-1}(s)H_0(s)\eta_r(s)$.

Lemma 1 If the filter $F(s)$ is designed such that it verifies the condition in (38), then the closed-loop reference system in equations (40) and (41) is BIBS stable with respect to the reference input and initial conditions.

The proof is similar to the proof given in Section3.2.3 of [21].

The following Lemma states a preliminary results in order to show uniform boundedness of the prediction error.

Lemma 2 There exists a real $\mu > 0$, such that

$$\mu\|\tilde{x}\|^2 \leq \sigma^\top\sigma,$$

where μ is defined later.

Proof

Let P be a positve definite matrix solution of the Lypaunove equation

$$A_m P + PA_m{}^\top = -Q, \tag{42}$$

where $Q > 0$ is a Hermitian matrix.

For the case of SISO systems, using Theorem 1.1 in [33], on generalization of the Kantorovich inequality, we have

$$\frac{(\lambda\tilde{x})^2}{(\tilde{x}^\top P^{-1}\tilde{x})\,(\lambda P\lambda^\top)} \geqslant \frac{4}{\kappa + 2 + \kappa^{-1}}, \tag{43}$$

where $\kappa = \frac{\lambda_{max}(P)}{\lambda_{min}(P)}$ in the particular case of $\phi = 0$ [33], and $\lambda_{min}(P) > 0$, $\lambda_{max}(P) > 0$ are the minimum and maximum eigenvalues of P, respectively.

Therefore

$$\frac{4}{\kappa + 2 + \kappa^{-1}}\left(\tilde{x}^\top P^{-1}\tilde{x}\right)\left(\lambda P\lambda^\top\right) \leq \sigma^2. \tag{44}$$

Given a fundamental property of quadratic forms it can be written

$$\frac{4}{\kappa+2+\kappa^{-1}}\frac{\lambda_{min}(P)}{\lambda_{max}(P)}\|\tilde{x}\|^2\|\lambda\|^2 \leq \sigma^2, \tag{45}$$

given that $\lambda_{min}(P^{-1}) = \frac{1}{\lambda_{max}(P)}$. Defining $\alpha_1 = \frac{4}{\kappa+2+\kappa^{-1}}\frac{\lambda_{min}(P)}{\lambda_{max}(P)}\|\lambda\|^2$, it follows that

$$\alpha_1\|x\|^2 \leq \sigma^2. \tag{46}$$

To show the proof in case of MIMO systems, the matrix $\lambda \in \mathbb{R}^{m\times n}$ is partitioned as

$$\lambda = \begin{bmatrix} \lambda_1 \\ \vdots \\ \lambda_m \end{bmatrix}, \tag{47}$$

where $\lambda_i \in \mathbb{R}^{1\times n}, i = 1...m$. The sliding surface can also be written as

$$\sigma = \begin{bmatrix} \sigma_1 \\ \vdots \\ \sigma_m \end{bmatrix}, \tag{48}$$

where $\sigma_i \in \mathbb{R}, i = 1...m$.

Consequently, it is straightforward to write the vectorial case of (46) as:

$$\alpha_i\|x\|^2 \leq \sigma_i^2, i = 1...m, \tag{49}$$

where $\alpha_i = \frac{4}{\kappa_i+2+\kappa_i^{-1}}\frac{\lambda_{min}(P)}{\lambda_{max}(P)}\|\lambda_i\|^2$ and $\kappa_i = \frac{\lambda_{max}(P)}{\lambda_{min}(P)}\frac{1+\sin\phi_i}{1-\sin\phi_i}$.

Given

$$\sum_k^n(\alpha_i)\|x\|^2 \leq \sum_1^m \sigma_i^2 = \sigma^\top\sigma, \tag{50}$$

it follows that

$$\mu\|x\|^2 \leq \sigma^\top\sigma, \tag{51}$$

where $\mu = \sum_k^n \alpha_i$ and the proof is complete. □

In the following, it is shown that the prediction error $\tilde{x}(t)$, and the estimation errors of the disturbances, their bounds and the unknown parameters are uniformly bounded.

Lemma 3 The following bound holds for the norm of the prediction error

$$\|\tilde{x}\|_{\mathcal{L}_\infty} \leq \delta = \frac{\rho_0}{\Gamma\mu}, \tag{52}$$

where ρ_0 is defined later.

Furthermore, the prediction error $\tilde{x}(t)$ converges to zero, i.e.,

$$\lim_{t\to\infty}\tilde{x}(t) = 0. \tag{53}$$

Proof. In this section, the dependence of the parameters on (t) is dropped unless it is not clear from the context.

From (29) and (30), the prediction error dynamics can be written

$$\dot{\tilde{x}} = A_m\tilde{x} + B\tilde{\omega}u + \tilde{\eta}. \tag{54}$$

Consider the Lyapunov function candidate

$$V = \frac{1}{2}\sigma^\top\sigma + \frac{1}{2}\Gamma^{-1}\Big(\mathrm{tr}\big(\tilde{\omega}^\top\tilde{\omega}\big) + \tilde{L}_1^2 + \tilde{L}_2^2\Big). \tag{55}$$

Its derivative is given by

$$\dot{V} = \sigma^\top\dot{\sigma} + \Gamma^{-1}\Big(\mathrm{tr}\big(\tilde{\omega}^\top\dot{\tilde{\omega}}\big) + \tilde{L}_1\dot{\tilde{L}}_1 + \tilde{L}_2\dot{\tilde{L}}_2\Big). \tag{56}$$

From (31) and (54) the derivative of the sliding surface can be written

$$\dot{\sigma} = \lambda A_m\tilde{x} + \lambda B\tilde{\omega}u + \lambda\tilde{\eta}. \tag{57}$$

Replacing in (56), it follows that

$$\begin{aligned}\dot{V} =&\sigma^\top\Big(\lambda A_m\tilde{x} + \lambda B\tilde{\omega}u + \lambda(\hat{\eta}-\eta)\Big)\\ &+\Gamma^{-1}\big(\mathrm{tr}\big(\tilde{\omega}^\top\dot{\tilde{\omega}}\big) + \tilde{L}_1\dot{\tilde{L}}_1 \ + \tilde{L}_2\dot{\tilde{L}}_2\big).\end{aligned} \tag{58}$$

Given the fact that for any scalar s, $\mathrm{tr}(s) = s$, hence

$$\begin{aligned}\dot{V} =&\sigma^\top\lambda A_m\tilde{x} + \mathrm{tr}(\sigma^\top\lambda B\tilde{\omega}u) + \sigma^\top\lambda(\hat{\eta}-\eta)\\ &+\Gamma^{-1}\big(\mathrm{tr}\big(\tilde{\omega}^\top\dot{\tilde{\omega}}\big) + \tilde{L}_1\dot{\tilde{L}}_1 \ + \tilde{L}_2\dot{\tilde{L}}_2\big).\end{aligned} \tag{59}$$

Using the property $\mathrm{tr}(M_1; M_2) = \mathrm{tr}(M_2\ M_1)$ for any matrices M_1, M_2, we obtain

$$\begin{aligned}\dot{V} =&\sigma^\top\lambda A_m\tilde{x} + \mathrm{tr}(\tilde{\omega}u\sigma^\top\lambda B) + \sigma^\top\lambda(\hat{\eta}-\eta)\\ &+\Gamma^{-1}\big(\mathrm{tr}\big(\tilde{\omega}^\top\dot{\tilde{\omega}}\big) + \tilde{L}_1\dot{\tilde{L}}_1 \ + \tilde{L}_2\dot{\tilde{L}}_2\big).\end{aligned} \tag{60}$$

Given $\hat{\eta}$ (32) and the adaptation law (34) it can be written

$$\begin{aligned}\dot{V} =& -\rho\sigma^\top\lambda\tilde{x} - \sigma^\top\lambda\eta - \|\sigma^\top\lambda\|\big(\hat{L}_1\|x\|_\infty + \hat{L}_2\big)\\ &+\Gamma^{-1}\tilde{L}_1\dot{\tilde{L}}_1 + \tilde{L}_2\dot{\tilde{L}}_2.\end{aligned} \tag{61}$$

Hence, the following upper bound can be derived

$$\begin{aligned}\dot{V} \leq& -\rho\|\sigma\|^2 + \|\sigma^\top\lambda\|\|\eta\| - \|\sigma^\top\lambda\|\big(\hat{L}_1\|x\|_\infty + \hat{L}_2\big)\\ &+\Gamma^{-1}\tilde{L}_1\dot{\tilde{L}}_1 + \tilde{L}_2\dot{\tilde{L}}_2.\end{aligned} \tag{62}$$

Using the bound of η from assumption 5, it follows that

$$\begin{aligned}\dot{V} \leq& -\rho\|\sigma\|^2 - \|\lambda^\top\sigma\|\big(\tilde{L}_1\|x\|_\infty + \tilde{L}_2\big)\\ &+\Gamma^{-1}\tilde{L}_1\dot{\tilde{L}}_1 + \tilde{L}_2\dot{\tilde{L}}_2.\end{aligned} \tag{63}$$

Considering the adaptation law from (33), it follows that

$$\dot{V} \leq -\rho\|\sigma\|^2 < 0. \tag{64}$$

Therefore, the sliding surface σ, the estimation errors of the unknown parameter $\tilde{\omega}$; and the disturbance bounds errors $\tilde{L}_1$ and $\tilde{L}_2$ are uniformly bounded. Consequently, the estimation error of the external disturbance $\tilde{\eta}$ is also uniformly bounded.

Furthermore, from Lemma 2, we have:

$$\begin{aligned}\frac{1}{2}\mu\|x(t)\|^2 &\leq \frac{1}{2}\sigma(t)^\top\sigma(t)\\ &\leq V(t)\\ &\leq V(0) = \frac{1}{2}\Gamma^{-1}\Big(\mathrm{tr}\big(\tilde{\omega}(0)^\top\tilde{\omega}(0)\big) + \tilde{L}_1(0)^2 + \tilde{L}_2(0)^2\Big).\end{aligned} \tag{65}$$

Consequently the following upper bound holds

$$\|x\|^2 \leq \frac{\rho_0}{\Gamma\mu} \tag{66}$$

where $\rho_0 = \mathrm{tr}\big(\tilde{\omega}(0)^\top\tilde{\omega}(0)\big) + \tilde{L}_1(0)^2 + \tilde{L}_2(0)^2$.

Since $\|\cdot\|_\infty \leq \|\cdot\|$ and this bound is uniform, the bound above yields

$$\|\tilde{x}_\tau\|_{\mathcal{L}_\infty} \leq \sqrt{\frac{\rho_0}{\Gamma\mu}},$$

which holds for every $\tau \geq 0$, and leads to the uniform bound in (52).

Moreover, using (64) it can be written

$$\int_0^t \dot{V}(\tau)d\tau = V(t) - V(0) \leq -\int_0^t \rho\sigma^\top(\tau)\sigma(\tau)d\tau \tag{67}$$

Hence

$$V(t) + \int_0^t \rho\sigma^\top(\tau)\sigma(\tau)d\tau \leq V(0). \tag{68}$$

Since $V(0)$ is bounded and $V(t)$ is a non-increasing bounded function, it follows that

$$\lim_{t\to\infty}\int_0^t \rho\sigma^\top(\tau)\sigma(\tau)d\tau < \infty. \tag{69}$$

According to Barbalat's lemma [34,35], it can be concluded that

$$\lim_{t\to\infty} \rho\sigma^\top(\tau)\sigma(\tau)d\tau = 0, \tag{70}$$

which means that

$$\lim_{t\to\infty} \sigma(t) = 0 \tag{71}$$

and

$$\lim_{t\to\infty} \tilde{x}(t) = 0, \tag{72}$$

and the proof is complete. □

Remark 5. Similarly to the $\mathcal{L}_1$ adaptive control with gradient decent adaptation, the error uniform bound can be made arbitrarily small using large values of the adaptation rate Γ. The advantage using the sliding mode adaptation is that it can show the formal proof of asymptotic convergence of the prediction error and the performance bounds as we can see in the following theorem.

Theorem Given the system in (29), the reference system (40) and (41) and the $\mathcal{L}_1$ adaptive controller (30) to (35), then

$$\|x\|_{\mathcal{L}_\infty} \leq \rho, \quad \|u\|_{\mathcal{L}_\infty} \leq \rho_u,$$
$$\|x_{\mathrm{ref}} - x\|_{\mathcal{L}_\infty} \leq \gamma_1, \quad \|u_{\mathrm{ref}} - u\|_{\mathcal{L}_\infty} \leq \gamma_2.$$

The proof is similar to that given in Section 3.2.3 of [21].

5. Simulation Results

In this section, simulation results for the $\mathcal{L}_1$ adaptive controller are presented. The performance of the $\mathcal{L}_1$ adaptive controller was compared with the Adaptive Integral Backstepping (AIB) based path-following controller proposed in [36, 37]. The dynamics of the inner-loop controller are assumed to be robust against wind. The considered full airship model is from [38].

In the implementation of the $\mathcal{L}_1$ adaptive controller, the following parameters were set:

$$K = 2\,\mathbb{I}_3,\ D(s) = \frac{1}{s}\mathbb{I}_3,\ \lambda = \begin{bmatrix}0 & -1 & 0 & -1\\ 0 & 0 & -1 & 0\\ 1 & 0 & 0 & 0\end{bmatrix}$$

A state-feedback matrix K_p was computed by the Linear Quadratic Regulator (LQR) method to obtain the desired closed-loop system dynamics matrix A_m.

The airspeed of the airship V_a is assumed to be regulated at 20m/s.

The performance of the controller was evaluated without wind, with time-varying wind and with constant wind.

The results show that both controllers give a satisfactory performance when there are no wind disturbances. The trajectories of the airship and the path-following errors relative to the desired path are shown in Fig. 4. The trajectories are smooth and precise and are almost not distinguishable from the references. The $\mathcal{L}_1$ adaptive controller shows relatively better performance for both transient and steady state errors.

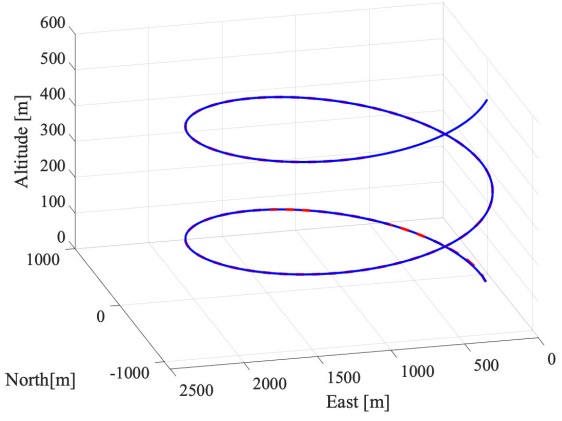

(a) $\mathcal{L}_1$ adaptive controller (Desired blue).

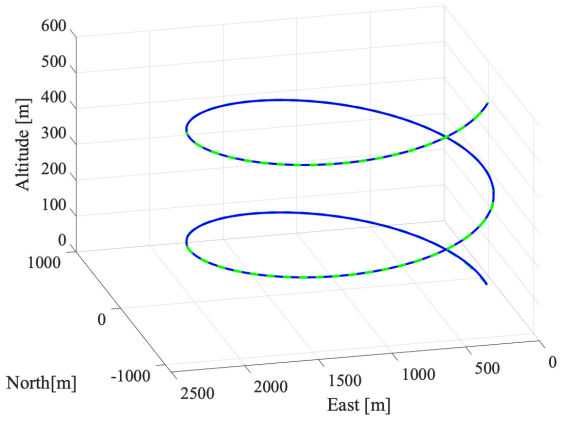

(b) AIB controller (Desired blue).

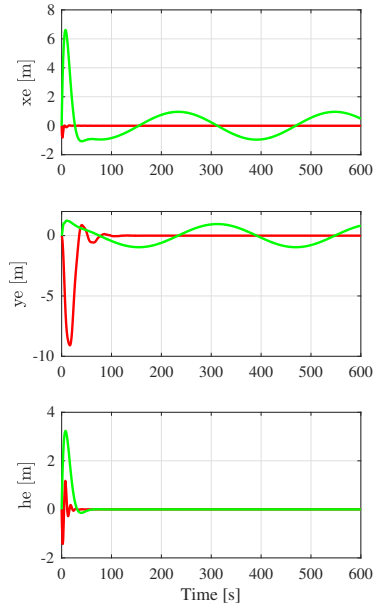

(c) Trajectories errors ($\mathcal{L}_1$ red, AIB green).

Fig. 4. Airship trajectories and errors without wind

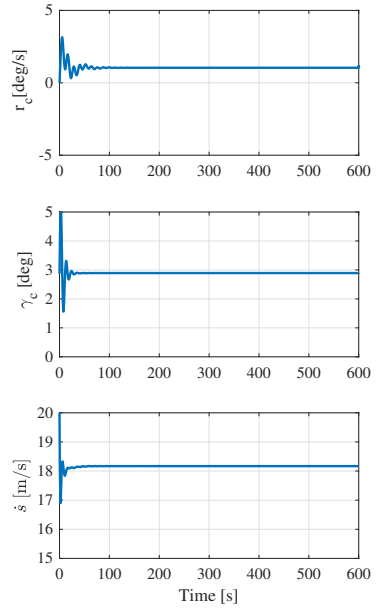

(a) Output commands $\mathcal{L}_1$ adaptive controller.

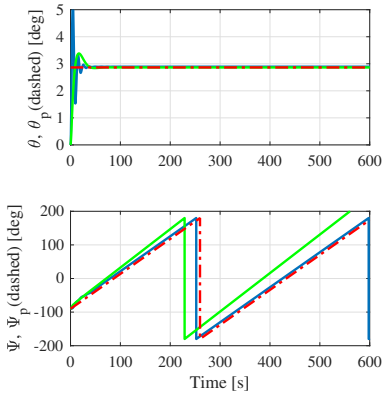

(b) Desired and actual angles ($\mathcal{L}_1$ blue, AIB green).

Fig. 5. Simulation parameters without wind

The output commands of the $\mathcal{L}_1$ adaptive controller, the speed of virtual target and the orientation of the airship are illustrated in Fig. 5. It can be observed that the $\mathcal{L}_1$ adaptive controller has produced smooth commands. The commands of the AIB controller are not shown because they are based on the computation of the velocity and the attitudes [36, 37], and they cannot be fairly compared to the commands of the $\mathcal{L}_1$ adaptive controller.

In the second test, a time-varying is introduced at simulation time $t = 60$s, with a velocity that is assumed to be a periodic signal $[0, 3 + 3\sin(0.2\pi t), 3 + 3\sin(0.2\pi t)]^\top$ m/s.

It is shown in Fig. 6 that the AIB controller is not able to keep the airship on the desired path, whereas, as expected, the $\mathcal{L}_1$ adaptive controller performs better and maintains the airship on the nominal trajectory.

As it can be observed from Fig. 6c, the maximal long-track error x_e, cross-track error y_e and altitude error z_e, are within reasonable limits, considering that this wind condition is extreme for an airship.

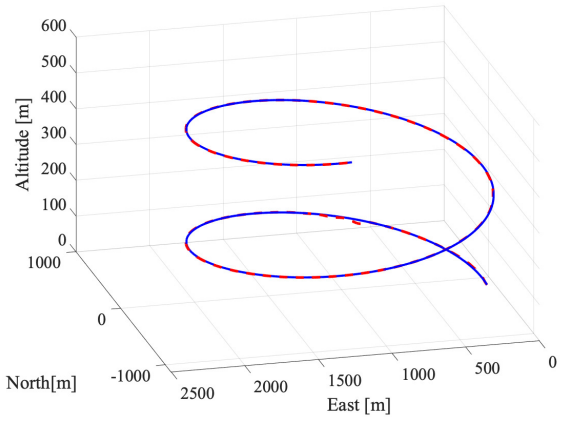

(a) $\mathcal{L}_1$ adaptive controller (Desired blue).

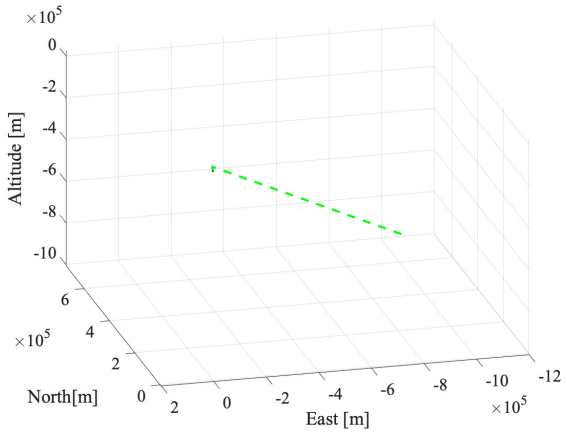

(b) AIB controller .

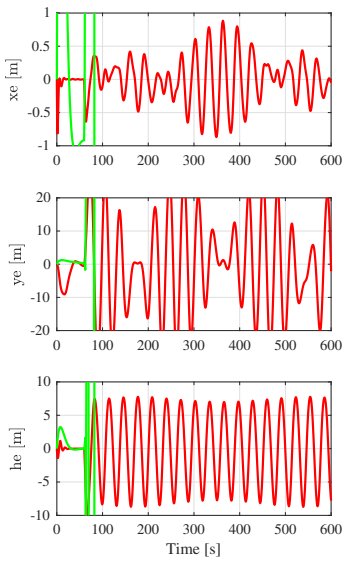

(c) Trajectories errors ($\mathcal{L}_1$ red, AIB green).

Fig. 6. Airship trajectories and errors in wind

Furthermore, it can be noticed in Fig. 7a that the commands of the yaw rate r_c and path angle γ_c are produced to counteract the wind disturbance. It can also be noted that the speed of the virtual target is accelerated or decelerated as necessary.

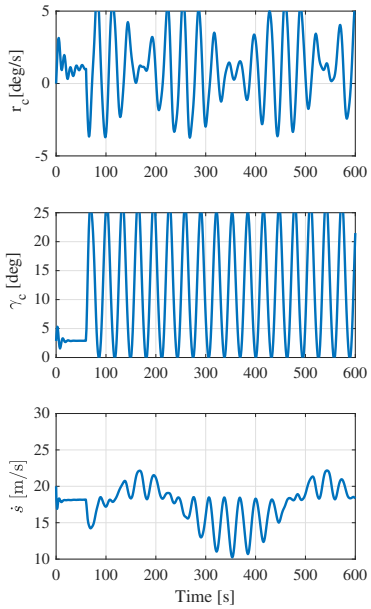

(a) Output commands $\mathcal{L}_1$ adaptive controller.

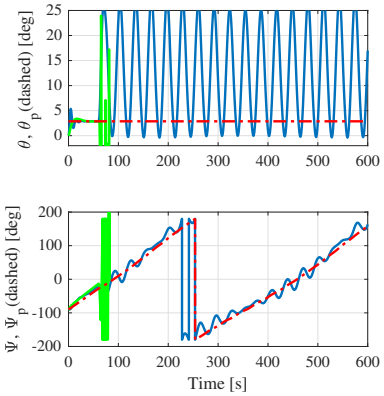

(b) Trajectories errors ($\mathcal{L}_1$ blue, AIB green).

Fig. 7. Simulation results in wind

Next, a constant wind is introduced, blowing with a velocity vector of $[0, 6, 6]^\top$m/s. In Fig. 8a, it can be seen that the trajectory of the airship is smooth and precise in these relatively extreme wind conditions. From the data presented in Fig. 8b, it is evident that the altitude error z_e has been eliminated entirely. Additionally, the maximal long-track error x_e and cross-track error y_e are relatively small, even though the airship is operating under extreme wind conditions.

As shown in Fig.9, the residual errors in x_e and y_e are due to the periodic nature of the trajectory reference

for a helix path. It is well established that state-feedback systems can have relatively poor reference tracking performance, which contributes to these residual errors. It has been demonstrated in a simulation case of straight-line path-following that the tracking errors x_e, y_e, and z_e converge actually to zero, as shown in Fig. 10.

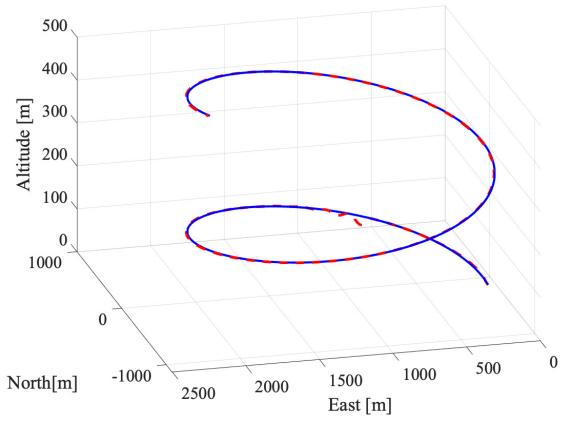

(a) $\mathcal{L}_1$ adaptive controller (Desired blue).

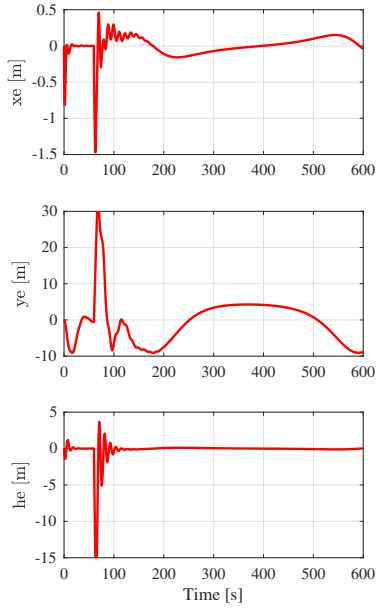

(b) Trajectories errors.

Fig. 8. Simulation results for helix path in constant wind

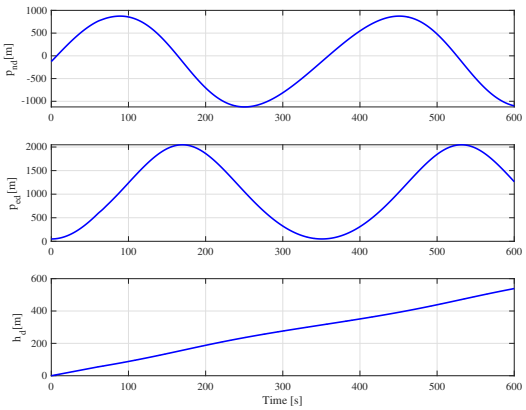

Fig. 9. Reference trajectories

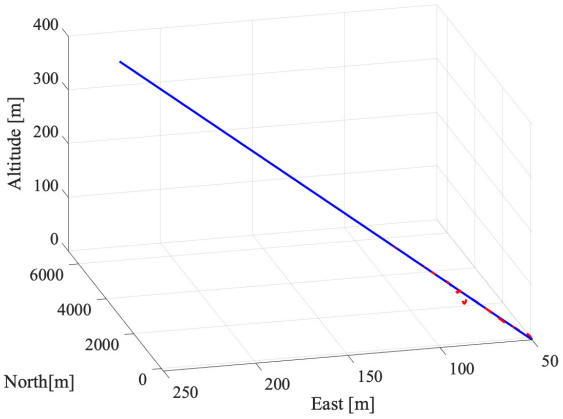

(a) Airship 3D trajectory (Desired blue).

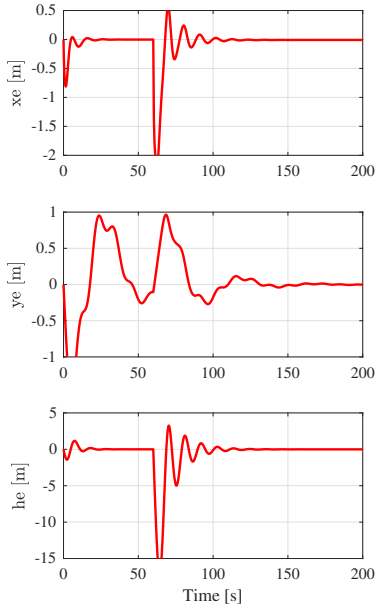

(b) Trajectories errors

Fig. 10. Simulation results for straight-line path in constant wind

These simulations demonstrate that the designed $\mathcal{L}_1$ adaptive path-following controller shows good performance in wind conditions. This is due to its robustness and fast adaptation in the presence of external disturbances.

6. Summary

An approach for adaptive 3D path-following by an airship is presented in this paper. General three dimensional curved paths are considered. The design is based on the control of the motion of the airship towards a virtual target. The main idea is to formulate path following of airships as a control design for systems in the presence of parametric uncertainties and external disturbances. Assuming that wind is time-varying, the proposed solution is based on sliding mode $\mathcal{L}_1$ adaptive control. At the same time the controller provides the desired vehicle attitude and the commanded speed of the virtual target. The proposed approach makes clear statements for performance specifications of the controller and relaxes the common assumption that the wind speed is constant. Simulation results are presented that validate the efficacy and efficiency of the proposed controller.

The formulation of airship path-following as a problem of control design in the presence of uncertainties and external disturbances opens a gap for the introduction of a large panel of control methodologies for the development of robust path-following in wind. Future research can also investigate the design based on cascaded $\mathcal{L}_1$ adaptive architecture, while the attitude controller is based on $\mathcal{L}_1$ adaptive control.

References

[1] A.-U. Haque, W. Asrar, A. A. Omar and E. Sulaeman, Defining reference area for prediction of aerodynamic coefficients of a biologically inspired hybrid buoyant vehicle, *Unmanned Systems* **5**(04) (2017) 237–246.

[2] F. Khoshnoud, I. I. Esat, C. W. de Silva, J. D. Rhodes, A. A. Kiessling and M. B. Quadrelli, Self-powered solar aerial vehicles: towards infinite endurance UAVs, *Unmanned Systems* **8**(02) (2020) 95–117.

[3] Z.-P. Jiang and H. Nijmeijer, A recursive technique for tracking control of nonholonomic systems in chained form, *IEEE Transactions on Automatic Control* **44**(2) (1999) 265–279.

[4] Y. Wang, W. Zhou, J. Luo, H. Yan, H. Pu and Y. Peng, Reliable intelligent path following control for a robotic airship against sensor faults, *IEEE/ASME Transactions on Mechatronics* **24**(6) (2019) 2572–2582.

[5] C. Altafini, Following a path of varying curvature as an output regulation problem, *IEEE Transactions on Automatic Control* **47**(9) (2002) 1551–1556.

[6] J. R. Azinheira, E. C. de Paiva and S. S. Bueno, Influence of wind speed on airship dynamics, *Journal of Guidance, Control, and Dynamics* **25**(6) (2002) 1116–1124.

[7] Q. Tao, T. J. Tan, J. Cha, Y. Yuan and F. Zhang, Modeling and control of swing oscillation of underactuated indoor miniature autonomous blimps, *Unmanned Systems* **9**(01) (2021) 73–86.

[8] Winds in the stratosphere and mesosphere `https://www.britannica.com/science/climate-meteorology/Winds-in-the-stratosphere-and-mesosphere`, Accessed: 2020-12-30.

[9] J. R. Azinheira, E. C. de Paiva, J. Ramos and S. Beuno, Mission path following for an autonomous unmanned airship, *Proceedings 2000 ICRA. Millennium Conference. IEEE International Conference on Robotics and Automation. Symposia Proceedings*, **2** (2000), pp. 1269–1275.

[10] D. Schmidt, Dynamic modeling, control and station-keeping guidance of a large high-altitude near-space airship, *AIAA Guidance, Navigation, and Control Conference and Exhibit*, (2006), p. 6781.

[11] Z. Zheng and Z. Wu, Global path following control for underactuated stratospheric airship, *Advances in Space Research* **52**(7) (2013) 1384–1395.

[12] Z. Zheng and W. Huo, Planar path following control for stratospheric airship, *IET Control Theory & Applications* **7**(2) (2013) 185–201.

[13] J. R. Azinheira, A. Moutinho and E. C. de Paiva, A backstepping controller for path-tracking of an underactuated autonomous airship, *International Journal of Robust and Nonlinear Control: IFAC-Affiliated Journal* **19**(4) (2009) 418–441.

[14] Z. Zuo, L. Cheng, X. Wang and K. Sun, Three-dimensional path-following backstepping control for an underactuated stratospheric airship, *IEEE Transactions on Aerospace and Electronic Systems* **55**(3) (2018) 1483–1497.

[15] X. Wang, Z. Zuo and C. Liu, Three dimensional path-following control of an under-actuated airship, *2016 35th Chinese Control Conference (CCC)*, IEEE (2016), pp. 4627–4632.

[16] A. Moutinho, J. R. Azinheira, E. C. de Paiva and S. S. Bueno, Airship robust path-tracking: A tutorial on airship modelling and gain-scheduling control design, *Control Engineering Practice* **50** (2016) 22–36.

[17] Y. Wei, P. Zhou, Y. Wang, D. Duan and Z. Chen, Virtual guidance-based finite-time path-following control of underactuated autonomous airship with error constraints and uncertainties, *Proceedings of the Institution of Mechanical Engineers, Part G: Journal of Aerospace Engineering* (2020) p. 0954410020969319.

[18] W. X. Zhou, P. F. Zhou, Y. Y. Wang and D. P. Duan, Planar path following nonlinear controller design for an autonomous airship, *Proceedings of the Institution of Mechanical Engineers, Part G: Journal of Aerospace Engineering* **233**(5) (2019) 1879–1899.

[19] L. Cheng, Z. Zuo, J. Song and X. Liang, Robust three-dimensional path-following control for an underactuated stratospheric airship, *Advances in Space Research* **63**(1) (2019) 526–538.

[20] J. Wang, X. Meng and G. Wu, Path following of the autonomous airship with compensation of unknown wind and modeling uncertainties, *Aerospace Science and Technology* **93** (2019) p. 105349.

[21] N. Hovakimyan and C. Cao, $\mathcal{L}_1$ *Adaptive Control Theory: Guaranteed Robustness with Fast Adaptation* (Siam, 2010).

[22] V. Dobrokhodov, E. Xargay, N. Hovakimyan, I. Kaminer, C. Cao and I. M. Gregory, Multicriteria analysis of an $\mathcal{L}_1$ adaptive flight control system, *Proceedings of the Institution of Mechanical Engineers, Part I: Journal of Systems and Control Engineering* **227**(4) (2013) 413–427.

[23] D. Xu, J. F. Whidborne and A. Cooke, Fault tolerant control of a quadrotor using $\mathcal{L}_1$ adaptive control, *Int. J. Intell. Unmanned Syst.* **4**(1) (2016) 43–66.

[24] Y. Zhou, H. Liu, H. Guo and X. Duan, $\mathcal{L}_1$ adaptive dynamic inversion attitude control for unmanned aerial vehicle with actuator failures, *Proceedings of the Institution of Mechanical Engineers, Part G: Journal of Aerospace Engineering* **233**(11) (2019) 4129–4140.

[25] T. Souanef, $\mathcal{L}_1$ adaptive output feedback control of small unmanned aerial vehicles, *Unmanned Systems* (2022) 1–12.

[26] T. Souanef, $\mathcal{L}_1$ adaptive path-following of small fixed-wing unmanned aerial vehicles in wind, *IEEE Transactions on Aerospace and Electronic Systems* **58**(4) (2022) 3708–3716.

[27] T. Souanef, Adaptive guidance and control of small unmanned aerial vehicle, PhD thesis, University of Stuttgart, Germany (2019).

[28] R. W. Beard and T. W. McLain, *Small Unmanned Aircraft: Theory and Practice* (Princeton University Press, 2012).

[29] M. Breivik and T. I. Fossen, Principles of guidance-based path following in 2D and 3D, *Proceedings of the 44th IEEE Conference on Decision and Control*, IEEE (2005), pp. 627–634.

[30] A. Micaelli and C. Samson, Trajectory tracking for unicycle-type and two-steering-wheels mobile robots, tech. rep., INRIA (1993).

[31] E. Lavretsky and K. A. Wise, Robust adaptive control, *Robust and Adaptive Control*, (Springer, 2013), pp. 317–353.

[32] T. Souanef, A. Boubakir and W. Fichter, $\mathcal{L}_1$ adaptive control of systems with disturbances of unknown bounds, *Advances in Aerospace Guidance, Navigation and Control: Selected Papers of the Third CEAS Specialist Conference on Guidance, Navigation and Control held in Toulouse*, Springer (2015), p. 151.

[33] J. Huang and J. Zhou, A direct proof and a generalization for a Kantorovich type inequality, *Linear Algebra and its Applications* **397** (2005) 185–192.

[34] I. Barbalat, Systemes d'équations différentielles d'oscillations non linéaires, *Rev. Roumaine Math. Pures Appl.* **4**(2) (1959) 267–270.

[35] J.-J. E. Slotine, W. Li *et al.*, *Applied Nonlinear Control* (Prentice-Hall Englewood Cliffs, NJ, 1991).

[36] S. Liu and Y. Sang, Underactuated stratospheric airship trajectory control using an adaptive integral backstepping approach, *Journal of Aircraft* **55**(6) (2018) 2357–2371.

[37] S. Q. Liu, J. F. Whidborne and L. He, Backstepping sliding-mode control of stratospheric airships using disturbance-observer, *Advances in Space Research* **67**(3) (2021) 1174–1187.

[38] J. Mueller, M. Paluszek and Y. Zhao, Development of an aerodynamic model and control law design for a high altitude airship, *AIAA 3rd Unmanned Unlimited Technical Conference, Workshop and Exhibit*, (2004), p. 6479.